Improved Energy Management Strategy for Prosumer Buildings with Renewable Energy Sources and Battery Energy Storage Systems

Pavitra Sharma, *Student Member*, *IEEE*, Krishna Kumar Saini, *Student Member*, *IEEE*, Hitesh Datt Mathur, *Senior Member*, *IEEE*, and Puneet Mishra, *Member*, *IEEE*

***Abstract*—The concept of utilizing microgrids (MGs) to convert buildings into prosumers is gaining massive popularity because of its economic and environmental benefits. These prosumer buildings consist of renewable energy sources and usually install battery energy storage systems (BESSs) to deal with the uncertain nature of renewable energy sources. However, because of the high capital investment of BESS and the limitation of available energy, there is a need for an effective energy management strategy for prosumer buildings that maximizes the profit of building owner and increases the operating life span of BESS. In this regard, this paper proposes an improved energy management strategy (IEMS) for the prosumer building to minimize the operating cost of MG and degradation factor of BESS. Moreover, to estimate the practical operating life span of BESS, this paper utilizes a non-linear battery degradation model. In addition, a flexible load shifting (FLS) scheme is also developed and integrated into the proposed strategy to further improve its performance. The proposed strategy is tested for the real-time annual data of a grid-tied solar photovoltaic (PV) and BESS-powered AC-DC hybrid MG installed at a commercial building. Moreover, the scenario reduction technique is used to handle the uncertainty associated with generation and load demand. To validate the performance of the proposed strategy, the results of IEMS are compared with the well-established energy management strategies. The simulation results verify that the proposed strategy substantially increases the profit of the building owner and operating life span of BESS. Moreover, FLS enhances the performance of IEMS by further improving the financial profit of MG owner and the life span of BESS, thus making the operation of prosumer building more economical and efficient.**

***Index Terms*—Prosumer building, battery energy storage system (BESS), battery degradation factor, demand response, energy management, microgrid, solar photovoltaic (PV) system.**

Manuscript received: October 6, 2023; revised: December 12, 2023; accepted: February 8, 2024. Date of CrossCheck: February 8, 2024. Date of online publication: March 30, 2024.

This work was supported in part by the Department of Science and Technology, Government of India, New Delhi, India "Internet of Things (IoT) Research of Interdisciplinary Cyber-Physical Systems Program" (No. DST/ICPS/CLUSTER/IoT/2018/General).

P. Sharma (corresponding author), K. K. Saini, H. D. Mathur, and P. Mishra are with Department of Electrical & Electronics Engineering, Birla Institute of Technology & Science, Pilani, India (e-mail: sharmapavitra334@gmail. com; krishnasaini16@gmail.com; mathurhd@pilani.bits-pilani.ac.in; puneet.mishra@pilani.bits-pilani.ac.in).

DOI: 10.35833/MPCE.2023.000761

I. Introduction

As fossil fuel-based energy resources have significantly harmed the environment, the growth of solar power has steadily emerged as a key strategy for advancing the transition to low-carbon energy [1]-[3]. However, with increased large-scale solar power installation, the need for energy storage technology has significantly increased [4], [5]. Therefore, energy storage systems are becoming critical technological components of today's power grid infrastructure. Recently, battery energy storage systems (BESSs) have been deployed for a variety of grid applications, ranging from their installation at the generation site to the end-user site [6]. Their features such as fast response, storage and provision of energy when needed (time shifting), and adaptable installation capabilities due to the modularization of their cell structure have made them more popular and advantageous [7], [8]. Because of the mentioned features, BESSs can have a wide range of power and energy capabilities. Hence, they balance the uncertain nature of renewable energy sources, especially in microgrid (MG) scenarios.

The life span of BESS is mainly determined by various components such as depth of discharge (DOD), charging/discharging cycles, and environmental conditions [9]. For any of the BESS applications, maximizing the DOD reduces the energy storage capacity and thus increases the number of cycles. Further, the degradation factor of BESS mainly depends on its energy exchange, which, in turn, diminishes battery capacity (i.e., capacity fading) [10]. Although the ageing mechanism of batteries is complex, for optimal scheduling, parameters such as DOD and charging/discharging cycles have the most significant influence on degradation. The number of cycles of BESS is defined as the maximum number of charging/discharging cycles allowed to a BESS. The BESS is considered thoroughly degraded when its number of cycles reaches its maximum value or its energy capacity is reduced to a predetermined level (for example, 80% of rated capacity). The maximum number of cycles for a particular battery type is determined from the experimental data [11]. Therefore, it varies depending on its manufacturer.

Aside from applications of BESSs in large and interconnected power systems, many small-scale systems including households, buildings, localities, or even factories have re-

cently employed their BESSs [12] - [14]. These are major electricity consumers and are incentivized to incorporate renewable energy generation and BESSs into their energy system to create a new class of flexible and effective prosumers. Moreover, prosumer buildings can attain substantial economic profit if they optimally manage their energy production, consumption, and the energy they exchange with the power grid. However, because of the high capital investment of the BESS and the limited amount of available energy due to its state of charge (SOC), there is a need for an effective energy management strategy for prosumer buildings that aims at economical and efficient operation of MGs. The economic operation leads to the minimization of the operating cost of MG, and efficient operation deals with improving the active life span of BESS.

With the increased popularity of BESSs, their integration into the MG network has significantly increased. Therefore, various studies have been conducted on MG energy management and its optimal operation, considering different generation sources and storage systems [15]-[21].

In [17], distributed economic dispatch is performed for a grid-connected MG with high renewable energy penetration and demand-side management. The developed algorithm aims to minimize the net cost of MG including the utility of dispatchable loads, cost of distributed generation and storage units, and worst-case transaction costs stemming from the uncertainty in renewable energy sources. Reference [18] develops an efficient energy management system for a solar photovoltaic (PV), wind, fuel cell, and battery energy scheme to minimize the operation cost of the MG and maximize the power generated by each source. In [19], an energy management algorithm is formulated, which is based on a mixed-integer linear programming (MILP) problem for grid-connected and islanded MGs integrated with solar PV, wind, fuel cell, microturbine, diesel generator, and BESS to minimize the operating cost. Reference [20] develops a home energy management system consisting of solar PV, battery, and the power grid. It aims to lower the operating cost of the system and maximize the green factor. The proposed management system could decrease the cost objective by 17% and significantly improve the performance ratio. An energy management system for a grid-connected MG consisting of solar PV and BESS is proposed in [21] to minimize the operating cost by controlling battery charging/discharging operations based on the load of MG.

These studies focus on minimizing the operating cost of MG, but do not focus on reducing battery degradation. In this paper, these studies are termed as conventional energy management strategy (CEMS).

In addition to the above-mentioned points, various studies have developed energy management strategies for MG considering battery degradation [22] - [29]. In [22] and [23], a linear model of the battery degradation cost is considered that assumes a proportional relationship with the amount of energy exchanged by the battery, regardless of the charging discharging cycle depth and the current SOC level. In [24], a unit commitment model is formulated that aims at cost minimization considering the battery degradation model based on cycle depth. Reference [25] proposes a regression-based battery degradation cost model that considers the temperature and cycle depth of the battery, i.e., DOD. However, these studies do not consider the current SOC of each cycle.

Further, in [26] and [27], piece-wise linearization of the life cycle function (number of cycles vs. DOD) is proposed for the sizing of BESS in an under-planning MG to achieve the convexity of the formulated problem. References [28] and [29] use the rainflow cycle counting algorithm based on the piecewise approximation model of battery degradation. A novel battery degradation model is developed in [11] that uses the concept of auxiliary SOC of the battery with the cycle depth, and formulates a cost minimization objective function. However, piece-wise linear approximation is used to incorporate the battery degradation model into an optimization problem. These energy management strategies considering battery degradation in the optimization model are termed as existing energy management strategy (EEMS) for further use in this paper.

It is worth mentioning that all aforementioned studies use piece-wise linear approximation to linearise the life cycle function of BESS, and some ignore calendar ageing that significantly governs the operating life span of BESS. Therefore, these models fail to depict the practical degradation and estimation of the operating life span of BESS.

In this regard, there is a need to design an energy management strategy for an MG that incorporates a realistic BESS life span estimation model based on static and dynamic degradation, and is independent of linear approximation of life cycle function. Further, it should also consider the generation and load uncertainties, resulting in lower operating cost of MG and improved the operating life span of BESS.

In order to showcase the limitations of the above-mentioned literature, Table I presents the summary of energy management strategies for MGs presented in the literature.

In view of the limitations of previously reported energy management strategies and identified research gaps, an attempt has been made through this paper to address these shortcomings. The major contributions of this paper are as follows:

1) A non-linear battery degradation model considering calendar and cyclic ageing in terms of static and dynamic degradation factors, respectively, is used to estimate the practical operating life span of BESS.

2) An improved energy management strategy (IEMS) is developed to maximize the profit of a prosumer building with an AC-DC hybrid MG by minimizing the operating cost of MG and improving the operating life span of BESS. It is achieved by minimizing the formulated cost objective function of MG as per the proposed rule-based algorithm (RBA). The proposed RBA decides the contribution of BESS and power grid based on solar PV power, load demand power, type of load demand (off-peak load/peak load), and SOC of BESS.

3) A flexible load shifting (FLS) scheme is formulated aiming at shifting the flexible loads from the time slot where the equivalent power (solar PV generation subtracted from the load power) is the maximum to the time slot where it is the minimum. The proposed FLS scheme is further integrated into the IEMS to improve its effectiveness in reducing the operating cost of MG and the degradation of BESS.

TABLE I
SUMMARY OF ENERGY MANAGEMENT STRATEGIES FOR MGS PRESENTED IN LITERATURE

Reference	Objective		Algorithm used	Type of battery degradation model and their limitations	Demand response	Method to handle uncertainty
	Minimization of cost	Minimization of battery degradation				
[17]	√	×	Robust optimization	N/A	√	Joint uncertainty model
[19]	√	×	Fuzzy interface with MILP	N/A	√	×
[21]	√	×	Rule-based algorithm with linear programming (LP)	N/A	×	Day-ahead forecasted data
[22]	√	√	RBA	DOD-independent linear model	×	Day-ahead forecasted data
[23]	√	√	Meta-heuristic optimization	DOD-independent linear model	×	×
[24]	√	√	Meta-heuristic optimization	DOD-dependent linear model without considering the current state of SOC	×	Robust optimization
[25]	√	√	Non-linear programming	DOD- and temperature-based regression model without considering current SOC	√	×
[27]	√	√	MILP	Piece-wise linearization model	×	Robust optimization
[28]	√	√	MILP	Rainflow cycle counting algorithm with further linearization	×	Data with forecasted error
[11]	√	√	MILP	DOD and auxiliary SOC-based piecewise linearized model	×	Model predictive control
This paper	√	√	RBA with meta-heuristic optimization	Purely non-linear degradation model considering both calendar and cyclic ageing	√	Real-time data and scenario reduction technique

The remainder of this paper is organized as follows. Section II discusses the configuration of AC-DC hybrid MG in prosumer building and its components. Section III presents the description of the non-linear degradation model of BESS and the estimation of its operating life span. Section IV discusses the development of the proposed IEMS with the formulation of the cost optimization model and FLS scheme. Section V presents the case studies and the results. This paper is concluded in Section VI.

II. CONFIGURATION OF AC-DC HYBRID MG IN PROSUMER BUILDING AND ITS COMPONENTS

This section details the configuration, specifications, and components of the studied system. Figure 1 shows the structure of AC-DC hybrid MG in the prosumer building. The AC-DC hybrid MG comprises a solar PV system, the maximum power point tracking (MPPT) charger, BESS, and a hybrid multimode bi-directional inverter. It is installed on the rooftop of a commercial building at a university campus. These components are detailed in the following subsections.

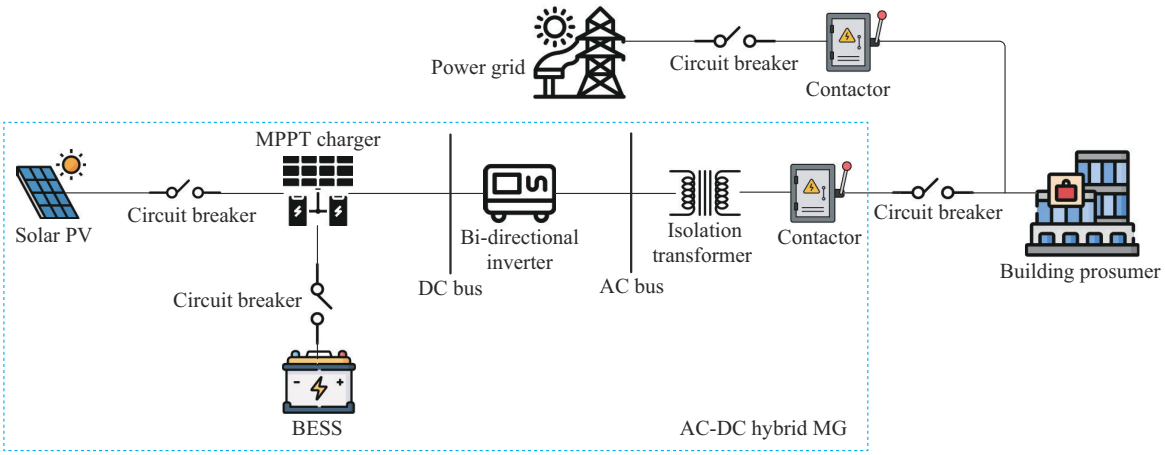

Fig. 1. Structure of AC-DC hybrid MG in prosumer building.

A. Solar PV System

The power of solar PV system is expressed in terms of solar irradiance and temperature using (1) [30].

$$P_{PV}^{t}=\eta_{PV}P_{PV}^{R}\frac{G_{m}^{t}}{G^{N}}\left[1+K_{Te}\left(Te_{A,m}^{t}-Te_{N}\right)\right]\quad\forall t\in T \tag{1}$$

where P_{PV}^{R} is the rated power of the PV generator; G_{m}^{t} is the measured solar radiation at time t; G^{N} is the nominal solar

radiation, which is assumed to be 1000 W/m^2; K_{Te} is a constant equal to –0.0357 ℃$^{-1}$; $Te^t_{A,m}$ is the measured ambient temperature at time t; Te_N is the panel temperature under standard test conditions, which is assumed to be 25 ℃; η_{PV} is the performance coefficient of the PV power converter; and T is the total number of time intervals.

The AC-DC hybrid MG has a solar PV rooftop system of 41.2 kWp, which consists of 77 solar PV panels. Each panel has a rated peak power of 535 Wp at normal operating cell temperature (NOCT). Figure 2 shows the solar PV panels and the AC-DC hybrid MG installed at a prosumer building.

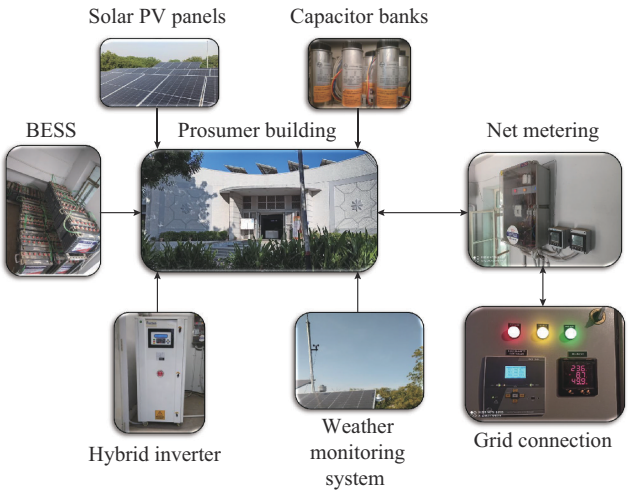

Fig. 2. AC-DC hybrid MG installed at a prosumer building with solar PV panels.

B. BESS

The BESS is mathematically modelled using (2) and (3) [31].

$$P^t_{B,ch}(\text{or } P^t_{B,Dch})=\begin{cases}P^t_B<0 & \text{charging}\\ P^t_B>0 & \text{discharging}\\ P^t_B=0 & \text{stand-by}\end{cases}\quad \forall t\in T \tag{2}$$

$$SOC^{t+1}_B=\begin{cases}SOC^t_B(1-\rho_B)-\dfrac{P^t_{B,Ch}\eta_{B,Ch}\Delta t}{E^R_B} & \text{charging}\\ SOC^t_B(1-\rho_B)-\dfrac{P^t_{B,Dch}}{\eta_{B,Dch}E^R_B}\Delta t & \text{discharging}\end{cases}\quad \forall t\in T \tag{3}$$

where $P^t_{B,Ch}$ and $P^t_{B,Dch}$ are the charging and discharging power of BESS at time t, respectively, and $P^t_{B,Ch}$ is always negative and $P^t_{B,Dch}$ is always positive; SOC^t_B and SOC^{t+1}_B are the SOCs of BESS at time t and $t+1$, respectively; ρ_B is the self-discharging rate of BESS; $\eta_{B,Ch}$ and $\eta_{B,Dch}$ are the charging and discharging efficiencies of BESS, respectively; and E^R_B is the rated energy capacity of BESS.

Moreover, the BESS operation is subject to the constraints (4)-(6).

$$0\ge P^t_{B,Ch}\ge P^{\max}_{B,Ch}\quad \forall t\in T \tag{4}$$

$$0\le P^t_{B,Dch}\le P^{\max}_{B,Dch}\quad \forall t\in T \tag{5}$$

$$SOC^{\min}_B\le SOC^t_B\le SOC^{\max}_B\quad \forall t\in T \tag{6}$$

where $P^{\max}_{B,Ch}$ and $P^{\max}_{B,Dch}$ are the maximum charging and discharging limits of BESS, respectively; and $SOC^{\min}_B$ and $SOC^{\max}_B$ are the minimum and maximum limits of the SOC of BESS, respectively.

The BESS of 81 kWh capacity is connected to the AC-DC hybrid MG using 30 lead acid (LA) batteries with rated values of 12 V/225 Ah @C20. They are connected in series; therefore, the rating of BESS becomes 360 V/225 Ah.

C. Load Demand of Prosumer Building

The load demand of the prosumer building has two components, i.e., flexible and non-flexible load demands. The flexible load demand can be shifted to any time slot, which can be represented by:

$$P^t_L=P^t_{FL}+P^t_{NFL}\quad \forall t\in T \tag{7}$$

where P^t_L is the load demand power of the prosumer building at time t; and P^t_{FL} and P^t_{NFL} are the flexible and non-flexible load power at time t, respectively. The load demand of the building varies as per the constraint in (8).

$$P^{\min}_L\le P^t_L\le P^{\max}_L\quad \forall t\in T \tag{8}$$

where $P^{\min}_L$ and $P^{\max}_L$ are the minimum and maximum limits of load demand, respectively.

D. Grid Power Modelling

The grid power flow P^t_G is bidirectional and is expressed by (9). The grid power acts as a source for the MG to satisfy the load demand, and as a sink when there is an excess renewable power generation.

$$\begin{cases}P^t_G>0 & \text{grid is exporting power to MG}\\ P^t_G<0 & \text{grid is importing power from MG}\end{cases}\quad \forall t\in T \tag{9}$$

The grid operation is restricted by the constraints discussed in (10) and (11).

$$0\le P^t_G\le P^{\max}_{G,Ex}\quad \forall t\in T \tag{10}$$

$$P^{\max}_{G,Im}\le P^t_G\le 0\quad \forall t\in T \tag{11}$$

where $P^{\max}_{G,Ex}$ and $P^{\max}_{G,Im}$ are the maximum limits of power exported to and imported from the grid, respectively.

III. Formulation of Non-linear Life Estimation Model of BESS

The battery life model has two aspects, i.e., calendar life and cycle life. The calendar life reflects the capacity decline over time (due to the passage of time) without taking into account the battery's cycles. It is affected by the factors surrounding the installation location of the battery, and is therefore considered as a non-operational factor. However, cycle life is determined by the maximum possible charging and discharging cycles of a battery. It is primarily determined by operational methods such as how often and how deeply the battery charges and discharges.

The degradation of battery life refers to the loss of life induced by the degradation of battery functional qualities and changes under operating conditions. In other words, battery degradation is stated as a percentage decrease in the life span of the battery. There are several factors that contribute to the degradation of battery life such as battery cycle time, charging/discharging status, temperature, and its operation

way. The battery degradation factor (BDf) is segregated into two components, i.e., static degradation (BDf_S) and dynamic degradation (BDf_D), and can be expressed by (12).

$$BDf = BDf_S + BDf_D \tag{12}$$

BDf_S is mainly caused by the deterioration of functional qualities of the battery such as the growth of a passivation layer on the negative electrodes, thickening of the electrolyte interface film, electrode active material loss, and electrolyte oxidation.

As a result of this functional feature degradation, the internal resistance of the battery will rise, which will reduce its capacity. It is considered linear with battery shelf life because it is independent of operating conditions. The annual static depreciation is expressed in (13) [10].

$$BDf_S = \frac{1}{T_S} \tag{13}$$

where T_S is the battery calendar/shelf life. For instance, if the battery calendar/shelf life is 12 years, the static degradation for one year is $1/12 = 8.33\%$.

BDf_D is completely associated with the operating conditions of the battery. Operating factors include the DOD and the charging/discharging rate, which correspond to the charging/discharging procedure of the battery. Because practical charging/discharging cycles are aperiodic, the dynamic deterioration becomes non-linear. Therefore, it is crucial to consider practical operating circumstances while calculating the dynamic degradation, as indicated by (14) [10].

$$BDf_D = \sum_{i=1}^{N} \frac{1}{C_{i(kl)}} \quad \forall i \in N \tag{14}$$

where i is the i^{th} charging/discharging cycle; k and l are the beginning and end of the charging/discharging process between SOC values SOC_k and SOC_l, respectively; N is the total number of charging/discharging intervals; and $C_{i(kl)}$ is the number of cycles when the battery is charged and discharged between k and l until its capacity falls to 60% of its nominal capacity, which is calculated using (15).

$$\frac{1}{C_{i(kl)}} = \frac{1}{2}\left(\frac{1}{C_{i(k)}} - \frac{1}{C_{i(l)}}\right) \quad \forall i \in N \tag{15}$$

where $C_{i(k)}$ and $C_{i(l)}$ are the cycle numbers when the SOC charges and discharges from SOC_k and SOC_l to 100%, respectively, in regard to the i^{th} charging/discharging cycle. Further, $1/C_{i(k)}$, $1/C_{i(l)}$, and $1/C_{i(kl)}$ are the dynamic degradations when the SOC charges from SOC_k to 100%, SOC_l to 100%, and SOC_k to SOC_l, respectively.

The dynamic degradation of battery for time T (BDf_D^T) can be expressed using (16) [10].

$$BDf_D^T = \sum_{t=1}^{T} BDf_D^t = \sum_{t=1}^{T}\sum_{i=1}^{N}\left|\frac{1}{2}\left(\frac{1}{C_{i(k)}} - \frac{1}{C_{i(l)}}\right)\right| \quad \forall t \in T, \forall i \in N \tag{16}$$

where BDf_D^t is the dynamic degradation for time interval t.

Based on (12)-(16), if $T = 8760$ hours $= Y$, the annual battery degradation factor BDf^Y becomes:

$$BDf^Y = \frac{1}{T_S} + \sum_{t=1}^{Y} BDf_D^t \quad \forall t \in Y \tag{17}$$

In order to estimate the accurate BDf for any battery, only the relationship between the number of cycles and its SOC or DOD needs to be examined. Thus, it is possible to compute battery degradation of any charging/discharging interval for practical operating conditions and estimate the total operating life span T_{OL} of any battery.

When the battery life degradation process reaches 100%, i.e., the battery degradation factor becomes unity, as shown in (18), the estimated T_{OL} can be determined.

$$\sum_{Y=1}^{T_{OL}} BDf^Y = 100\% \quad \forall Y \tag{18}$$

Figure 3 shows the flowchart for calculating T_{OL} of a battery.

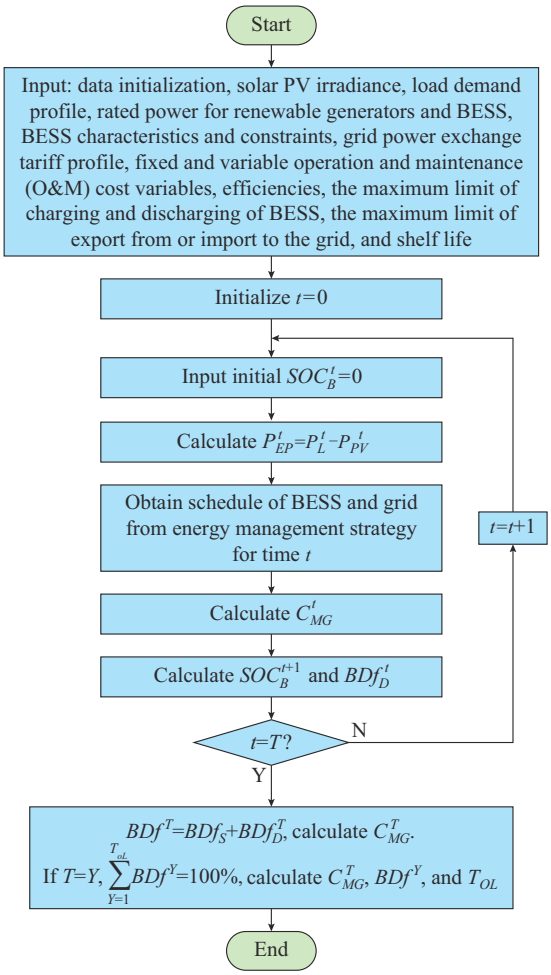

Fig. 3. Flowchart for calculating T_{OL} of a battery.

IV. Development of Proposed IEMS

This section discusses the proposed IEMS and FLS schemes and their integrations. The major objective of IEMS is to minimize the operating cost of the MG for the prosumer building and increase the operating life span of BESS. Moreover, the FLS scheme is developed to facilitate the IEMS in accomplishing the desired objectives.

A. Formulation of IEMS

In order to compensate for the limitations of the CEMS and EEMS of MG, this paper develops an IEMS. The salient features of IEMS are described as follows.

1) It aims to maximize the profit of the prosumer building by optimizing the operating cost associated with MG.

2) It focuses on improving the total operating life span of BESS by reducing its degradation factor and optimally utilizing solar PV generation.

3) It consists of an RBA that governs the operation of MG depending on four factors: solar PV power, load demand, type of load demand (off-peak/peak), and the current status of BESS.

4) The formulated RBA decides the contribution of BESS and grid, which depends on rules considering the above four factors as input.

To minimize the total operating cost of MG C_{MG}^{t}, a cost optimization model is formulated that considers the O&M cost of solar PV system, O&M cost model of complete BESS with variable and fixed cost terms, and cost associated with the grid power exchange. The formulated cost optimization model is shown in (19). The mathematical expressions of the components of the formulated model are presented in (20)-(22).

$$\min C_{MG}^{T}=\sum_{t=1}^{T}C_{MG}^{t}=\sum_{t=1}^{T}\zeta_{PV}^{O\&M}+\left|P_{B,Ch/Dch}^{t}\Delta t\right|\Phi_{B}^{O\&M}+\Psi_{B}^{O\&M}+P_{G}^{t}\lambda_{G}^{t}\Delta t\quad\forall t\in T \tag{19}$$

$$C_{PV}=\zeta_{PV}^{O\&M} \tag{20}$$

$$C_{B}^{t}=\left|P_{B,Ch/Dch}^{t}\Delta t\right|\Phi_{B}^{O\&M}+\Psi_{B}^{O\&M}\quad\forall t\in T \tag{21}$$

$$C_{G}^{t}=P_{G}^{t}\lambda_{G}^{t}\Delta t\quad\forall t\in T \tag{22}$$

where C_{MG}^{T} is the total operating cost of MG; C_{PV} is the hourly O&M cost of solar PV systems; C_{B}^{t} is the hourly O&M cost of BESS; C_{G}^{t} is the hourly cost of energy exchanged with the grid at time t; $\zeta_{PV}^{O\&M}$ is the O&M coefficient for the installed solar PV system; $P_{B,Ch/Dch}^{t}$ is charging/discharging power of BESS at time instant t; $\Phi_{B}^{O\&M}$ and $\Psi_{B}^{O\&M}$ are the variable and fixed O&M cost coefficients of BESS, respectively, and $\Phi_{B}^{O\&M}$ depends on $P_{B,Ch/Dch}^{t}$; P_{G}^{t} is the power exchanged with the grid at time t; and λ_{G}^{t} is the energy trading price of the grid at time t.

The formulated cost objective function is minimized subject to the constraints in (4)-(6), (10), (11), and (23).

$$P_{L}^{t}-P_{PV}^{t}-P_{B,Ch/Dch}^{t}-P_{G}^{t}=0\quad\forall t\in T \tag{23}$$

Figure 4 shows the flowchart of the proposed IEMS. The IEMS is a combination of an RBA and an optimization problem. For every time instant t, RBA takes the input of equivalent power P_{EP}^{t}, calculated using (24), average off-peak load demand $P_{L}^{Off\text{-}peak}$, and SOC of BESS at time t SOC_{B}^{t}. Based on these factors, it decides the BESS and grid status. When the $P_{EP}^{t}<0$, i.e., the generation exceeds the load demand, it prioritizes BESS to charge up to an SOC value threshold SOC_{TH}, and after this, the MG exports power to the grid. Further, for positive values of P_{EP}^{t}, i.e., the load demand is more than the generation, the contribution of BESS and grid to fulfill the unmet load demand is decided by the optimization problem. In the optimization problem, the variable discharging power of BESS $P_{B,Dch}^{t}$ has two bounds, i.e., lower and higher. For the lower bound, $P_{B,Dch}^{t}$ will remain between the limits 0 to $P_{B,Dch}^{\max}\beta$, whereas for the higher bound, it will vary between 0 to $P_{B,Dch}^{\max}$. Here, β is the constant that decides the contribution of BESS, which is taken as 0.85. This efficient utilization of BESS results in the reduction of the operating cost of MG as well as its degradation factor.

$$P_{EP}^{t}=P_{L}^{t}-P_{PV}^{t}\quad\forall t\in T \tag{24}$$

B. Formulation of FLS Scheme

Load shifting is a part of the load management technique in which the flexible loads are shifted to the off-peak hours from the peak hours of the day. The flexible loads can operate at any time of the day. Therefore, these loads are usually shifted as per the grid tariff or peak/off-peak load hours. However, in this paper, an FLS scheme is developed that performs the load shifting mechanism of flexible loads based on the equivalent power P_{EP}^{t} as it can give information on excess renewable generation and load unmet by renewable sources. Therefore, the FLS scheme focuses on shifting this unmet flexible load to the time instant where excess generation is available. It can minimize the burden on BESS and reduce the exported power to the MG, thereby decreasing the dynamic degradation of BESS and the operating cost of MG. After a thorough analysis, it is observed that most shiftable types of equipment are operated from 16:00 to 20:00. Also, the peak of load unmet by renewable sources occurs as the solar PV generation is low at this time. Therefore, it is desirable to shift these flexible types of equipment to the time slot where excess solar generation is available. Further, the flexible and non-flexible load power ratio is approximately 30%-35%. The FLS scheme is governed using the following steps.

Step 1: identify the time intervals with the minimum value (negative peak) of equivalent power and calculate the total excess solar PV power generation and its size.

Step 2: identify the time slots with the maximum value (positive peak) of equivalent power, and estimate the total flexible load power that can be shifted.

Step 3: select the time slots of the same size of flexible load power as that of excess solar generation. Calculate the total flexible load power to be shifted as per the excess solar generation power.

Step 4: move the flexible load on the selected time slot.

Implementing FLS scheme will change the daily load profile of the prosumer building, but the total load remains the same. To restrict the overpower at any time instant, constraint (8) must hold true, such as:

$$P_{L}^{\min}\le\hat{P}_{L}^{t}\le P_{L}^{\max}\quad\forall t\in T \tag{25}$$

where $\hat{P}_{L}^{t}$ is the load demand of the building obtained after the implementation of FLS scheme.

V. Case Study and Results

This section demonstrates in detail the effectiveness of IEMS over CEMS and EEMS. Further, the performance improvement of IEMS with FLS scheme is also discussed.

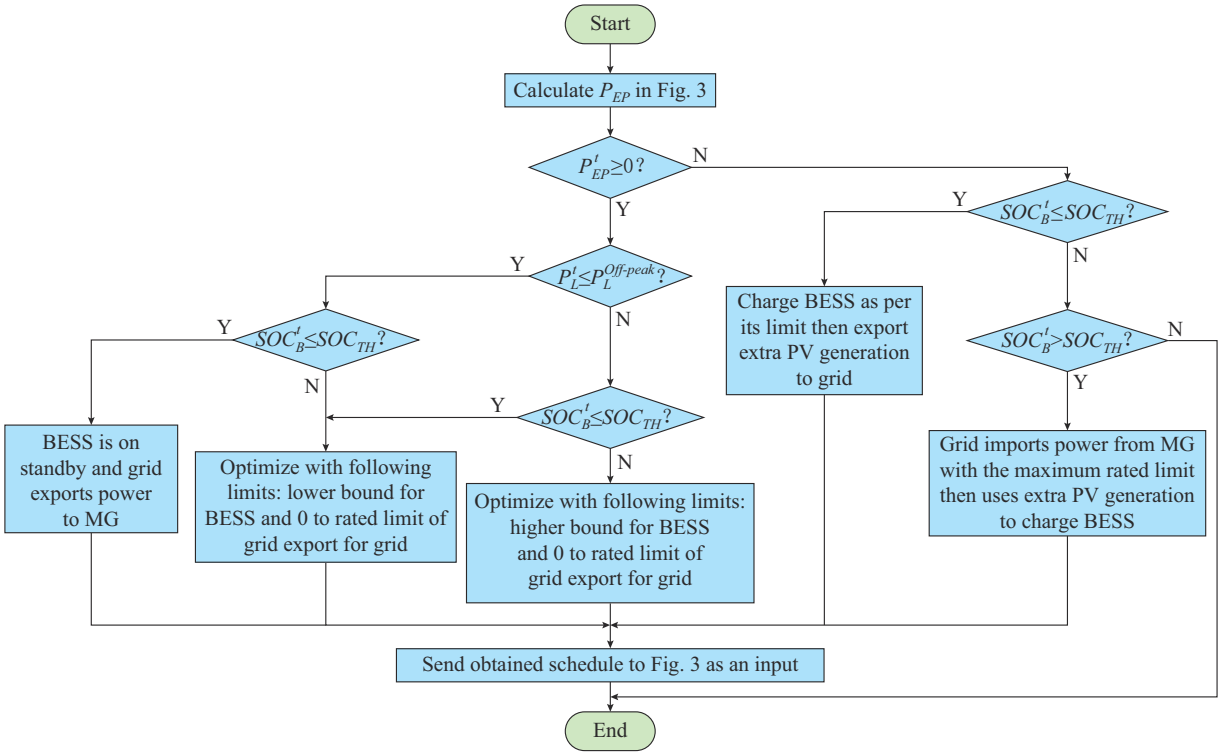

Fig. 4. Flow chart of proposed IEMS.

A. Input Data

In order to show the efficacy of IEMS, two time scales are considered. In Case 1, the performances of IEMS and IEMS+FLS over CEMS and EEMS are compared considering real-time data of the prosumer building for one year time scale. Figure 5(a) and (b) shows the real-time data of solar PV power and load demand for one year with 1 hour time step. The result for this scenario is analyzed and compared with different DOD levels, i.e., 30%, 50%, and 70%.

Further, in order to handle the uncertainty associated with solar PV generation and load demand and reduce the computational burden, the real-time data for one year are reduced to 10 scenarios using the scenario reduction technique [32], [33]. Thus, in Case 2, the performances of IEMS and IEMS+FLS over CEMS and EEMS are compared considering these scenarios, and further day-ahead scheduling is obtained. The result for this case is analyzed for 70% DOD level. Figure 6(a) and (b) shows the 10 solar PV power and load demand scenarios obtained using the scenario reduction technique. The solar PV power and load demand for Case 2 are expressed by (26) and (27), respectively. Figure 7 shows the day-ahead grid exchange prices with upper and lower bounds. More data can be found in [34].

$$P_{PV}^t = \sum_{s=1}^{S} \pi_{PV}^{t,s} P_{PV}^{t,s} \quad \forall s \in S \tag{26}$$

$$P_L^t = \sum_{s=1}^{S} \pi_L^{t,s} P_L^{t,s} \quad \forall s \in S \tag{27}$$

where S is the total number of scenarios; s is the index of a scenario; $P_{PV}^{t,s}$ and $P_L^{t,s}$ are the solar PV power and load demand of scenario s at time t, respectively; and $\pi_{PV}^{t,s}$ and $\pi_L^{t,s}$ are the probabilities of $P_{PV}^{t,s}$ and $P_L^{t,s}$, respectively.

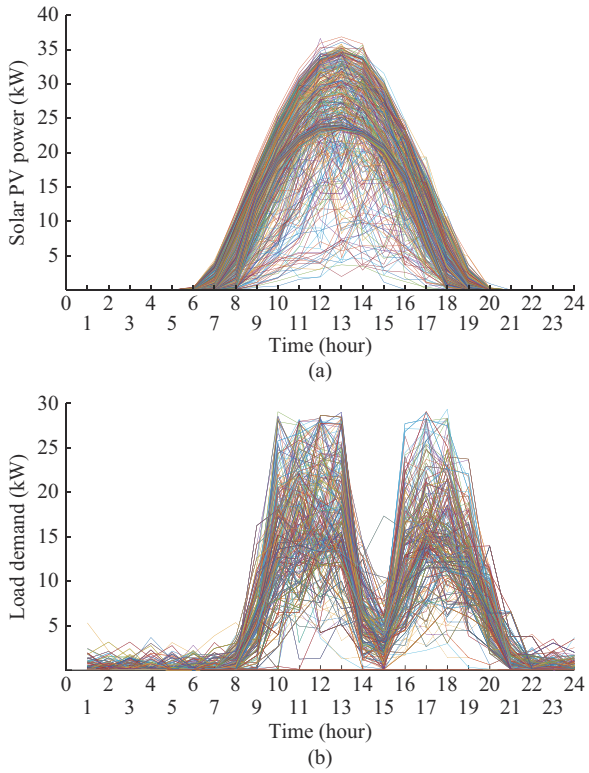

Fig. 5. Real-time data based 365 scenarios. (a) Solar PV power. (b) Load demand.

As discussed, the estimation of *BDf* for a battery depends on the relationship between the number of cycles and its SOC or DOD. Figure 8 shows the curve of the number of cycles (until battery capacity falls to 60% of its nominal capacity) vs. DOD of a LA battery with rated values of 12 V/225 Ah @C20 [35].

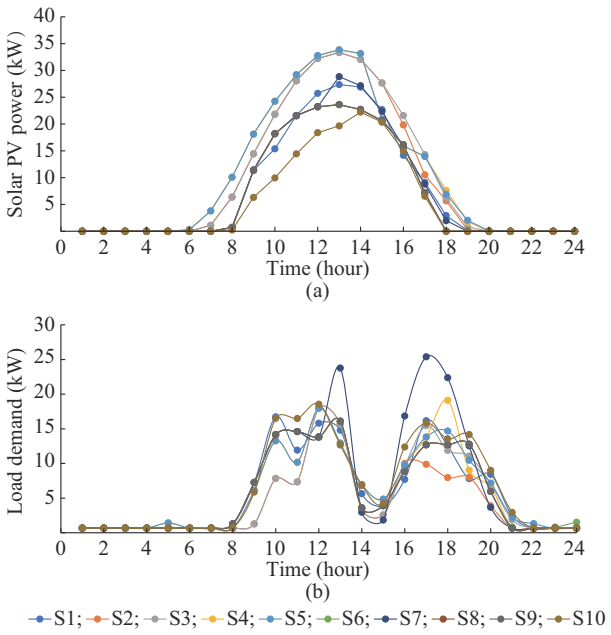

Fig. 6. Solar PV power and load demand obtained using scenario reduction technique. (a) Solar PV power. (b) Load demand.

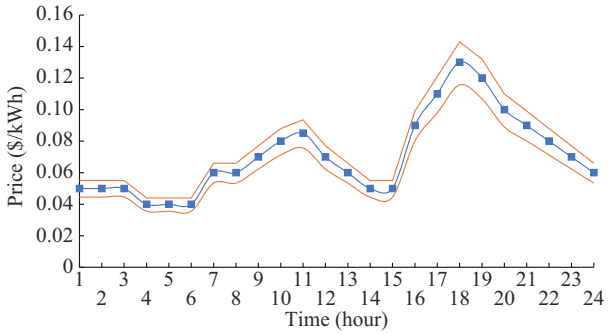

Fig. 7. Day-ahead grid exchange prices with upper and lower bounds.

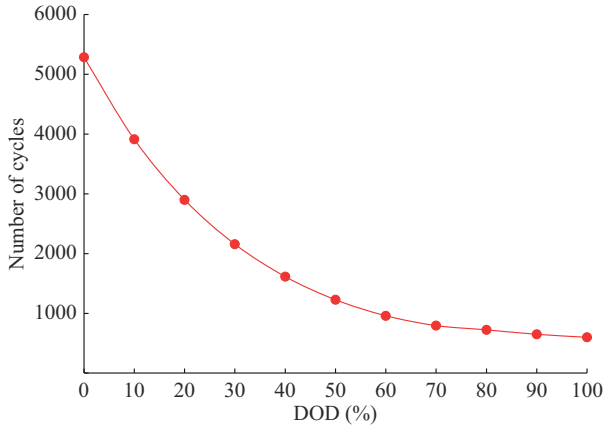

Fig. 8. Number of cycles (until battery capacity falls to 60% of its nominal capacity) vs. DOD of LA battery.

Using the curve fitting technique, a mathematical relationship between the number of cycles and DOD of LA battery is estimated as:

$$C_i^{LA,C20} = 5278.8\mathrm{e}^{-3.02DOD_i} + 5.894\mathrm{e}^{4.701DOD_i} \quad (28)$$

where C_i is the number of cycles at a DoD DOD_i defined as:

$$DOD_i = 1 - SOC_i \quad (29)$$

DOD_i means that the battery charges and discharges repeatedly between SOC_i and 100%. Therefore, using (29), the mathematical relationship between the number of cycles and SOC_i can be expressed as:

$$C_i^{LA,C20} = 5278.8\mathrm{e}^{-3.02(1-SOC_i)} + 5.894\mathrm{e}^{4.701(1-SOC_i)} \quad (30)$$

Table II presents the parameters used in the simulation obtained from the real-time MG installed at the prosumer building. Table III shows the cost coefficients of batteries and solar PV system. More data can be found in [35]-[38].

TABLE II
PARAMETERS USED IN SIMULATION

Scenario No.	Parameter	Value
1	$SOC_B^{\max}$	100%
2	$SOC_B^{\min}$ (depending on DOD)	70%, 50%, 30%
3	E_B^R	81 kWh
4	$P_{G,Ex}^{\max}$	35 kW
5	$P_{G,Im}^{\max}$	–17 kW
6	$P_{B,Ch}^{\max}, P_{B,Dch}^{\max}$	–4.05 kW, 4.05 kW
7	ρ_B	5% per month
8	$\eta_{B,Ch}, \eta_{B,Dch}$	0.85, 0.85
9	T_S	6 years
10	BDf_S	0.1666 per year

TABLE III
COST COEFFICIENTS OF BATTERIES AND SOLAR PV SYSTEM

$\Phi_B^{O\&M}$ ($/kWh)	$\Psi_B^{O\&M}$ ($/h)	$\zeta_{PV}^{O\&M}$ ($/h)
0.0005125	0.02854	0.057

B. Case 1: Performance Analysis of CEMS, EEMS, IEMS, and IEMS+FLS for a Year

This subsection presents the performance analysis of CEMS, EEMS, IEMS, and IEMS+FLS based on three major factors, i.e., the annual degradation factor, the total operating life span of BESS, and the annual operating cost of MG. The impact of change in DOD on MG operation is also analyzed.

Figures 9-11 show the annual operating cost of MG, the annual dynamic and static degradation factor, and the estimated total operating life span of BESS for CEMS, EEMS, IEMS, and IEMS+FLS, respectively, considering different DOD levels. The annual static degradation BDf_S of BESS only depends on the shelf life of BESS. Therefore, it is independent of the operational mode of MG and DOD levels of BESS. The lower value of the degradation factor results in a higher total operating life span of BESS.

Figures 9 and 10 show that IEMS has significantly reduced the operating cost of MG and dynamic degradation factor of BESS compared with CEMS and EEMS. Thus, the estimated total operating life span of BESS is higher for IEMS than for CEMS and EEMS, as shown in Fig. 11. Moreover, it is also noted that, as DOD increases, the dynamic degradation factor increases irrespective of the scheme, thereby decreasing the operating life span of BESS. This is due to the decrease in the number of cycles.

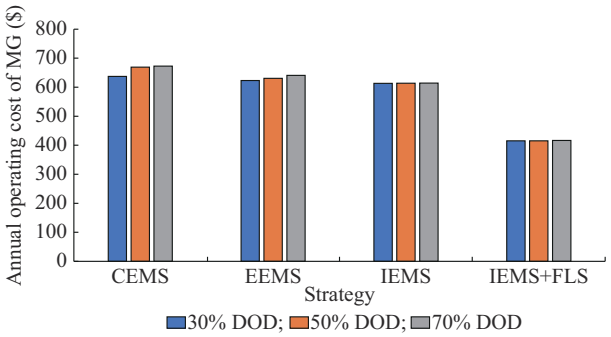

Fig. 9. Annual operating cost of MG for CEMS, EEMS, IEMS, and IEMS+FLS considering different DOD levels.

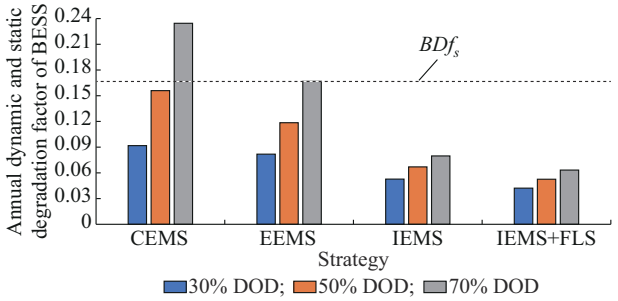

Fig. 10. Annual dynamic and static degradation factor of BESS for CEMS, EEMS, IEMS, and IEMS+FLS considering different DOD levels.

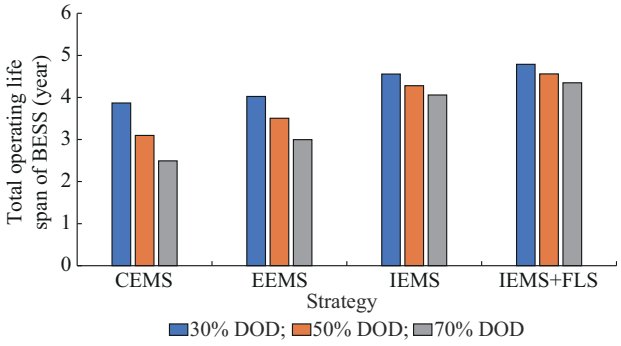

Fig. 11. Total operating life span of BESS for CEMS, EEMS, IEMS, and IEMS+FLS considering different DOD levels.

In addition, it can also be observed that the FLS scheme improves the performance of IEMS by further reducing the operating cost of MG and dynamic degradation factor and improving the total operating life span of BESS. By integrating FLS, the burden on BESS has been reduced, thereby decreasing its dynamic degradation factor and its O&M cost. Due to this, the total operating cost of MG reduces. Additionally, as the power exported by the grid decreases, the operating cost of MG is further reduced.

1) Impact of IEMS on Various Factors with Respect to CEMS

The percentage change in the annual operating cost of MG, annual dynamic degradation factor, and estimated total operating life span of BESS from IEMS with respect to CEMS is tabulated in Table IV. The negative and positive signs show the decrement and increment in the factor, respectively. Table IV shows that for the scenario of 70% DOD, there are 8.75% and 65.97% reductions in the operating cost of MG and degradation factor, respectively, and there is a 62.75% increment in the total operating life span of BESS. Thus, the profit earned by the prosumer building owner is significant in the case of IEMS in terms of cost and life span of BESS.

TABLE IV
PERCENTAGE CHANGE IN ANNUAL OPERATING COST OF MG, ANNUAL DYNAMIC DEGRADATION FACTOR, AND ESTIMATED TOTAL OPERATING LIFE SPAN OF BESS FROM IEMS WITH RESPECT TO CEMS

DOD level (%)	Percentage change in C^Y_{MG} (%)	Percentage change in BDf^Y_D (%)	Percentage change in T_{OL} (%)
30	−3.73	−42.46	17.75
50	−8.29	−57.06	38.10
70	−8.75	−65.97	62.75

2) Impact of IEMS on Various Factors with Respect to EEMS

Table V shows the percentage change in the annual operating cost of MG, annual dynamic degradation factor, and estimated total operating life span of BESS from IEMS with respect to EEMS. It can be observed that, for 70% of DOD, IEMS has decreased the operating cost and degradation of BESS by 4.17% and 52.16%, respectively, which is the highest among all DODs. Further, it improved the operating life span of BESS by 35.30% with respect to EEMS. Therefore, it can be concluded from Tables IV and V that IEMS is superior to CEMS and EEMS in terms of enhancing the profit of MG operator and improving the operating life span of BESS.

TABLE V
PERCENTAGE CHANGE IN ANNUAL OPERATING COST OF MG, ANNUAL DYNAMIC DEGRADATION FACTOR, AND ESTIMATED TOTAL OPERATING LIFE SPAN OF BESS FROM IEMS WITH RESPECT TO EEMS

DOD level (%)	Percentage change in C^Y_{MG} (%)	Percentage change in BDf^Y_D (%)	Percentage change in T_{OL} (%)
30	−1.54	−35.53	13.26
50	−2.68	−43.46	22.04
70	−4.17	−52.16	35.30

3) Impact of IEMS+FLS on Various Parameters with Respect to IEMS

The percentage change in the annual operating cost of MG, annual dynamic degradation factor and estimated total operating life span of BESS from IEMS+FLS with respect to IEMS is summarized in Table VI.

Table VI shows a considerable improvement in all the key factors by integrating IEMS and FLS. For 70% DOD, the decrease in operating cost and degradation factor is 32.38% and 20.67% from IEMS+FLS with respect to IEMS, respectively. Further, there is a 7.17% increment in the total operating life span of BESS. Therefore, it can be concluded that IEMS+FLS provides the maxi-

mum benefit to the prosumer building in terms of economic and efficiency perspectives.

TABLE VI
PERCENTAGE CHANGE IN ANNUAL OPERATING COST OF MG, ANNUAL DYNAMIC DEGRADATION FACTOR, AND ESTIMATED TOTAL OPERATING LIFE SPAN OF BESS FROM IEMS+FLS WITH RESPECT TO IEMS

DOD level (%)	Percentage change in C_{MG}^{Y} (%)	Percentage change in BDf_{D}^{Y} (%)	Percentage change in T_{OL} (%)
30	–32.31	–20.08	5.07
50	–32.34	–20.49	6.57
70	–32.38	–20.67	7.17

C. Case 2: Performance of CEMS, EEMS, IEMS, and IEMS+FLS for Day-ahead Optimal Scheduling

The performance analysis of CEMS, EEMS, IEMS, and IEMS+FLS considering reduced scenarios is discussed in this subsection. This analysis is performed for 70% DOD levels, as the higher DOD level is the most critical one. Figure 12 shows the day-ahead optimal scheduling of BESS and grid for CEMS, EEMS, and the proposed IEMS. Figure 13 also shows the SOC profile of BESS from CEMS, EEMS, and IEMS.

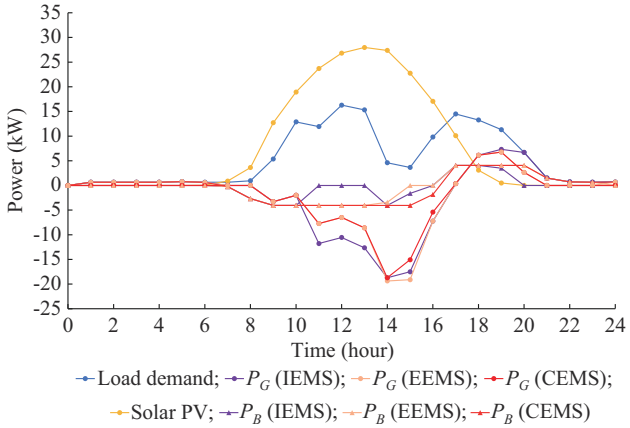

Fig. 12. Day-ahead optimal scheduling of BESS and grid for CEMS, EEMS, and IEMS.

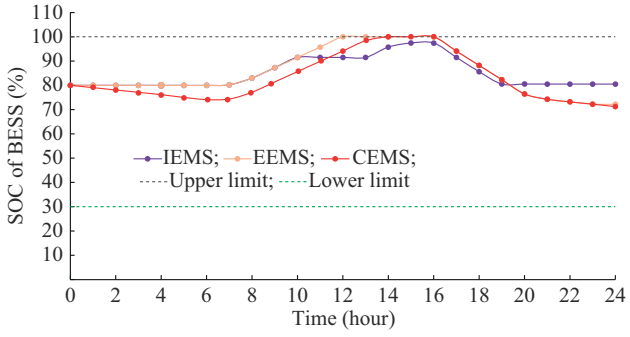

Fig. 13. SOC profile of BESS for CEMS, EEMS, and IEMS.

It can be observed that as the IEMS aims at optimal utilization of BESS, for time instants 10 and 11, when the BESS reaches to 90% SOC, it is not getting charged, due to which surplus generation is supplied to the grid and finally ends up reducing the operating cost of MG. When the equivalent power is positive, for time instant 20, after the peak hours, the BESS either discharges at a slightly lower rate than that of CEMS and EEMS or comes to a standby mode to decrease its degradation.

To estimate the efficacy of IEMS+FLS compared with IEMS, Fig. 14 shows the optimal day-ahead scheduling of BESS and grid for IEMS+FLS and IEMS. Moreover, Fig. 15 shows the SOC profile of BESS for IEMS+FLS and IEMS.

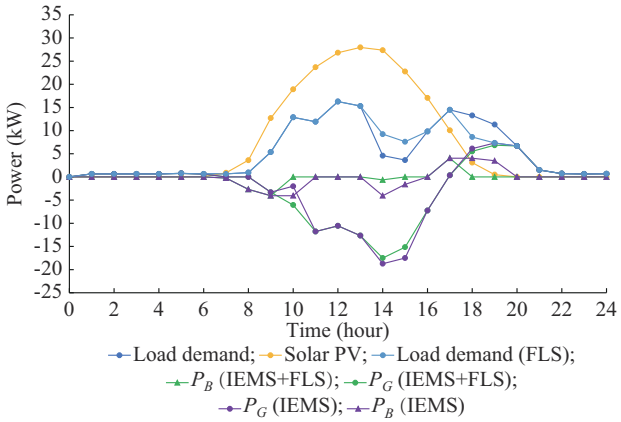

Fig. 14. Optimal day-ahead scheduling of BESS and grid for IEMS and IEMS+FLS.

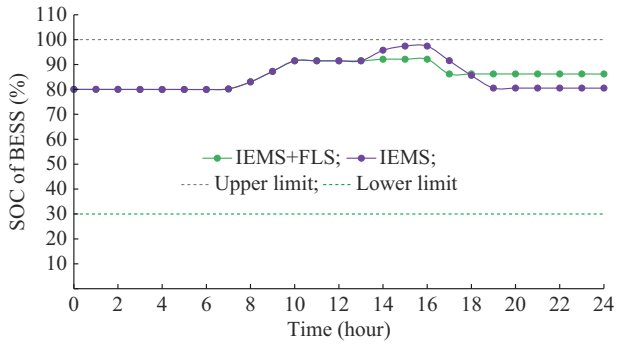

Fig. 15. SOC profile of BESS for IEMS and IEMS+FLS.

It can be observed from Fig. 14 that with the FLS scheme, the flexible load demand is shifted from the time slot where generation is less than the load to the time slot where excess generation is available. Further, due to this, the burden on BESS has been significantly reduced. Therefore, for time instants 18 and 19, the BESS discharges less than in IEMS, and net power exchange with the grid has also been reduced, as shown in Fig. 14.

The total operating cost of MG in one day and the dynamic degradation factor for CEMS, EEMS, IEMS, and IEMS+FLS are tabulated in Table VII. The negative sign in the total operating cost of MG shows the profit earned by the prosumer building owner. It can be noted from Table VII that the daily operating cost of MG and the dynamic degradation factor of BESS are the lowest for IEMS+FLS. Therefore, the proposed IEMS and IEMS+FLS can maximize the profit of the prosumer building owner and improve the operating life span of BESS compared with CEMS and EEMS.

TABLE VII
TOTAL OPERATING COST OF MG AND DYNAMIC DEGRADATION FACTOR OF BESS FOR CEMS, EEMS, IEMS, AND IEMS+FLS

Strategy	Total operating cost of MG C_{MG}^{T} (\$)	Dynamic degradation factor BDf_{D}^{T}
CEMS	–0.20	33.92×10^{-5}
EEMS	–0.38	24.73×10^{-5}
IEMS	–0.44	13.67×10^{-5}
IEMS+FLS	–0.73	5.29×10^{-5}

VI. CONCLUSION

This paper develops an IEMS for a prosumer building consisting of a solar PV and BESS-powered grid-tied AC-DC hybrid MG. The proposed strategy aims to maximize the building owner's profit by optimizing the operating cost of MG while simultaneously improving the total operating life span of BESS by reducing its degradation factor. It consists of an RBA, as per which the formulated objective function of MG is minimized. The proposed RBA decides the contribution of BESS and grid based on solar PV power, load demand power, type of load demand (off-peak/peak load), and condition of BESS. Moreover, this paper considers a non-linear battery degradation model that includes static and dynamic degradation factors to estimate the operating life span of BESS. Further, to improve the performance of the proposed strategy, an FLS scheme is developed that aims to effectively utilize solar PV generation to reduce the burden on BESS and thus reduce its degradation.

In Case 1, the proposed strategy is tested for one year with 1 hour time step. The data are obtained from grid-connected real-time MG consisting of a solar PV system and a BESS installed at a commercial building of a university campus. Further, to handle the uncertainty associated with solar PV generation and load demand and to reduce the computational burden, the scenario reduction technique is used to reduce these 365 scenarios to 10 scenarios. In Case 2, a day-ahead optimal scheduling is obtained using these reduced scenarios. The performance of the proposed strategy is validated by comparing the results of the strategy with the CEMS and EEMS of the MG. In order to showcase the effectiveness of IEMS, different DOD levels of BESS are considered, i.e., 30%, 50%, and 70%.

The results conclude that, for the critical DOD such as 70% and the yearly analysis, IEMS has reduced the operating cost of MG and the dynamic degradation of BESS by 4.17% and 52.16%, respectively, and increased the operating life span of BESS by 35.30% compared with EEMS. In addition, the FLS improves the efficacy of IEMS by further reducing the operating cost and degradation factor of BESS by 32.38% and 20.67% and enhancing the operating life span of BESS by 7.17%. Thus, the proposed strategy can be regarded as a superior energy management strategy for prosumer building in terms of improved economic profit and system efficiency by increasing the operating life span of BESS.

REFERENCES

[1] A. P. Arunkumar, S. Kuppusamy, S. Muthusamy *et al.*, "An extensive review on energy management system for microgrids," *Energy Sources, Part A: Recovery, Utilization, and Environmental Effects*, vol. 44, no. 2, pp. 4203-4228, May 2022.

[2] J. M. Raya-Armenta, N. Bazmohammadi, J. G. Avina-Cervantes *et al.*, "Energy management system optimization in islanded microgrids: an overview and future trends," *Renewable & Sustainable Energy Reviews*, vol. 149, p. 111327, Jun. 2021.

[3] P. Sharma, H. D. Mathur, P. Mishra *et al.*, "A critical and comparative review of energy management strategies for microgrids," *Applied Energy*, vol. 327, p. 120028, Oct. 2022.

[4] D. Zhang, H. Zhu, H. Zhang *et al.*, "Multi-objective optimization for smart integrated energy system considering demand responses and dynamic prices," *IEEE Transactions on Smart Grid*, vol. 13, no. 2, pp. 1100-1112, Nov. 2022.

[5] Y. Qiu, Q. Li, Y. Ai *et al.*, "Two-stage distributionally robust optimization-based coordinated scheduling of integrated energy system with electricity-hydrogen hybrid energy storage," *Protection and Control of Modern Power Systems*, vol. 8, no. 1, p. 33, Jul. 2023.

[6] P. Sharma, D. Bhattacharjee, H. D. Mathur *et al.*, "Novel optimal energy management with demand response for a real-time community microgrid," in *Proceedings of 2023 IEEE Industrial and Commercial Power Systems Europe (EEEIC/I&CPS Europe*), Madrid, Spain, Aug. 2023, pp. 1-6.

[7] J. F. Manwell and J. G. McGowan, "Lead acid battery storage model for hybrid energy systems," *Solar Energy*, vol. 50, no. 5, pp. 399-405, Aug. 2003.

[8] C. Goebel, H. Hesse, M. Schimpe *et al.*, "Model-based dispatch strategies for lithium-ion battery energy storage applied to pay-as-bid markets for secondary reserve," *IEEE Transactions on Power Systems*, vol. 32, no. 4, pp. 2724-2734, Nov. 2016.

[9] P. Sharma, P. Mishra, and H. D. Mathur, "Optimal energy management in microgrid including stationary and mobile storages based on minimum power loss and voltage deviation," *International Transactions on Electrical Energy Systems*, vol. 31, no. 12, p. e13182, Oct. 2021.

[10] G. Yan, D. Liu, J. Li *et al.*, "A cost accounting method of the Li-ion battery energy storage system for frequency regulation considering the effect of life degradation," *Protection and Control of Modern Power Systems*, vol. 3, no. 1, pp. 1-9, Feb. 2018.

[11] J. O. Lee and Y. S. Kim, "Novel battery degradation cost formulation for optimal scheduling of battery energy storage systems," *International Journal of Electrical Power & Energy Systems*, vol. 137, p. 107795, Nov. 2021.

[12] M. Rouholamini, C. Wang, H. Nehrir *et al.*, "A review of modeling, management, and applications of grid-connected Li-ion battery storage systems," *IEEE Transactions on Smart Grid*, vol. 13, no. 6, pp. 4505-4524, Jul. 2022.

[13] X. Li and S. Wang, "Energy management and operational control methods for grid battery energy storage systems," *CSEE Journal of Power and Energy Systems*, vol. 7, no. 5, pp. 1026-1040, Jun. 2021.

[14] S. Liu, C. Zhou, H. Guo *et al.*, "Operational optimization of a building-level integrated energy system considering additional potential benefits of energy storage," *Protection and Control of Modern Power Systems*, vol. 6, no. 1, p. 4, Feb. 2021.

[15] S. Suthar and N. M. Pindoriya, "Energy management platform for integrated battery-based energy storage-solar PV system: a case study," *IET Energy Systems Integration*, vol. 2, no. 4, pp. 373-381, Oct. 2020.

[16] P. K. Gayen, R. Majumdar, and S. Mondal, "Development and implementation of adaptive solar module- and battery characteristics-based real-time power management for solar battery system under grid-connected and islanded conditions," *International Journal of Electrical Power & Energy Systems*, vol. 30, no. 3, p. e12240, Nov. 2019.

[17] Y. Zhang, N. Gatsis, and G. B. Giannakis, "Robust energy management for microgrids with high-penetration renewables," *IEEE Transactions on Sustainable Energy*, vol. 4, no. 4, pp. 944-953, Sept. 2013.

[18] A. Elgammal and M. El-Naggar, "Energy management in smart grids for the integration of hybrid wind-PV-FC-battery renewable energy resources using multi-objective particle swarm optimization (MOPSO)," *The Journal of Engineering*, vol. 2018, no. 11, pp. 1806-1816, Nov. 2018.

[19] V. V. S. N. Murty and A. Kumar, "Multi-objective energy management in microgrids with hybrid energy sources and battery energy storage systems," *Protection and Control of Modern Power Systems*, vol. 5, no. 1, pp. 1-20, Jan. 2020.

[20] J. Zupančič, B. Filipič, and M. Gams, "Genetic-programming-based multi-objective optimization of strategies for home energy-management systems," *Energy*, vol. 203, p. 117769, Jul. 2020.
[21] R. J. J. Molu, S. R. D. Naoussi, P. Wira *et al.*, "Optimization-based energy management system for grid-connected photovoltaic/battery microgrids under uncertainty," *Case Studies in Chemical and Environmental Engineering*, vol. 8, p. 100464, Dec. 2023.
[22] X. Pan, R. Khezri, A. Mahmoudi *et al.*, "Energy management systems for grid-connected houses with solar PV and battery by considering flat and time-of-use electricity rates," *Energies*, vol. 14, no. 16, p. 5028, Aug. 2021.
[23] M. A. Hossain, H. R. Pota, S. Squartini *et al*., "Energy management of community microgrids considering degradation cost of battery," *Journal of Energy Storage*, vol. 22, pp. 257-269, Jun. 2019.
[24] A. R. Jordehi, "An improved particle swarm optimization for unit commitment in microgrids with battery energy storage systems considering battery degradation and uncertainties," *International Journal of Energy Research*, vol. 45, no. 1, pp. 727-744, Aug. 2021.
[25] M. F. Zia, E. Elbouchikhi, and M. Benbouzid, "Optimal operational planning of scalable DC microgrid with demand response, islanding, and battery degradation cost considerations," *Applied Energy*, vol. 237, pp. 695-707, Mar. 2019.
[26] M. Seydenschwanz, K. Majewski, C. Gottschalk *et al.*, "Linear approximation of cyclic battery aging costs for milp-based power dispatch optimization," in *Proceedings of 2019 IEEE PES Innovative Smart Grid Technologies Europe (ISGT-Europe)*, Bucharest, Romania, Sept. 2019, pp. 1-5.
[27] I. Alsaidan, A. Khodaei, and W. Gao, "A comprehensive battery energy storage optimal sizing model for microgrid applications," *IEEE Transactions on Power Systems*, vol. 33, no. 4, pp. 3968-3980, Jul. 2018.
[28] S. Cordova, C. Canizares, A. Lorca *et al.*, "An energy management system with short-term fluctuation reserves and battery degradation for isolated microgrids," *IEEE Transactions on Smart Grid*, vol. 12, no. 6, pp. 4668-4680, Nov. 2021.
[29] Y. Shi, B. Xu, Y. Tan *et al.*, "A convex cycle-based degradation model for battery energy storage planning and operation," in *Proceedings of 2018 Annual American Control Conference (ACC)*, Milwaukee, USA, Aug. 2018, pp. 4590-4596.
[30] K. Shivam, J. C. Tzou, and S. C. Wu, "A multi-objective predictive energy management strategy for residential grid-connected PV-battery hybrid systems based on machine learning technique," *Energy Conversion and Management*, vol. 237, no. 195, p. 114103, Jun. 2021.
[31] P. Hajiamoosha, A. Rastgou, S. Bahramara *et al.*, "Stochastic energy management in a renewable energy-based microgrid considering demand response program," *International Journal of Electrical Power & Energy Systems*, vol. 129, p. 106791, Jul. 2021.
[32] N. Gröwe-Kuska, H. Heitsch, and W. Römisch, "Scenario reduction and scenario tree construction for power management problems," in *Proceedings of 2003 IEEE Bologna PowerTech Conference*, Bologna, Italy, Jun. 2004, pp. 152-158.
[33] V. Singh, T. Moger, and D. Jena, "Uncertainty handling techniques in power systems: a critical review," *Electric Power Systems Research*, vol. 203, p. 107633, Feb. 2022.
[34] U. S. Energy Information Administration. (2022, Jun.). Grid electricity price. [Online]. Available: https://www.eia.gov/todayinenergy/prices.php
[35] Trojan Battery Company. (2019, Dec.). Data sheet of MODEL J185P-AC with Bayonet Cap MOTIVE J185P-AC. [Online]. Available: https://assets.ctfassets.net/nh2mdhlonj7m/cvlAE2cxiFyCxGCmQ2Fvu/648f13549334f1954d8e94bab0a23e9c/J185HAC_Trojan_Data_Sheets.pdf
[36] A. Walker, E. Lockhart, J. Desai *et al.* (2020, Jun.). Model of operation-and-maintenance costs for photovoltaic systems. [Online]. Available: https://www.nrel.gov/docs/fy20osti/74840.pdf
[37] A. Jäger-Waldau. (2019, Nov.). PV status report 2019. [Online]. Available: https://publications.jrc.ec.europa.eu/repository/handle/JRC118058
[38] K. Mongird, V. Viswanathan, J. Alam *et al.* (2020, Dec.). 2020 grid energy storage technology cost and performance assessment. [Online]. Available: https://www.pnnl.gov/sites/default/files/media/file/PSH_Methodology_0.pdf

Pavitra Sharma received the B.Tech. degree in power system engineering from University of Petroleum & Energy Studies (U.P.E.S.), Dehradun, India, and the M.E. degree in power system from Thapar Institute of Engineering & Technology (T.I.E.T.), Patiala, India, in 2017 and 2019, respectively. She is currently a Research Fellow at Birla Institute of Technology & Science (BITS), Pilani, India. Her research interests include power system optimization, energy management of microgrids, battery energy storage systems, and electric vehicle integration.

Krishna Kumar Saini received the B.Tech. degree in electrical engineering from Rajasthan Technical University (R.T.U.), Kota, India, and the M.Tech. degree in electrical & electronics engineering from Maharishi Dayanand University (M.D.U.), Rohtak, India, in 2013 and 2017, respectively. He is currently a Research Fellow at Birla Institute of Technology & Science (BITS), Pilani, India. His research interests include renewable resources integrated power system optimization, demand-side management, forecasting, and digital twin of microgrid.

Hitesh Datt Mathur received the B.E. degree in electrical engineering from Nagpur University, Nagpur, India, the M.E. degree in power systems from Malviya National Institute of Technology, Jaipur, India, and the Ph.D. degree from Birla Institute of Technology and Science (BITS), Pilani, India, in 1998, 2000, and 2007, respectively. He was a Postdoctoral Research Fellow at the Department of Automatic Control, Supelec, Gif-sur-Yvette, France. He is currently a Professor in the Department of Electrical and Electronics Engineering, Birla Institute of Technology & Science (BITS), Pilani, India, and Head of the School of Interdisciplinary Research and Entrepreneurship. His research interests include smart grid, internet-of-things (IoT)-based energy management, grid integration of renewable energy sources, e-mobility challenges, power quality analysis, and power system stability and control.

Puneet Mishra received the B.Tech. degree in electronics and instrumentation engineering from Uttar Pradesh Technical University, Lucknow, India, the M.E. degree in control and instrumentation engineering from Delhi College of Engineering, University of Delhi, New Delhi, India, and the Ph.D. degree from Netaji Subhas Institute of Technology, University of Delhi, New Delhi, India, in 2009, 2011, and 2017, respectively. He is currently working as an Assistant Professor in the Department of Electrical and Electronics Engineering, Birla Institute of Technology & Science (BITS), Pilani, India. His research interests include intelligent control for nonlinear systems, bio-inspired optimization, and integration of renewable energy sources in power system.